J Mater Sci: Mater Electron (2016) 27:9325–9334
DOI 10.1007/s10854-016-4972-9

Magnetoelectricity at room temperature in the $LaFeO_3/BiFeO_3$ heterostructures

M. G. Ranieri[1] · R. A. C. Amoresi[2] · M. A. Ramirez[1] · J. A. Cortes[1] · L. S. R. Rocha[1] · C. C. Silva[1] · A. Z. Simões[1]

Received: 18 February 2016 / Accepted: 9 May 2016 / Published online: 13 May 2016

Abstract Thin films of $BiFeO_3$ (BFO), $LaFeO_3$ (LFO), and LFO/BFO heterostructures were successfully obtained on $Pt/TiO_2/SiO_2/Si(100)$ substrates by chemical solution deposition. The films were characterized by structural, morphological and magneto-electrical techniques. The polycrystalline films obtained with good crystalline phases of BFO and LFO. The heterostructures films LFO/BFO showed no diffusion between the phases, and without the presence of secondary phases. The bottom layer of LFO was able to promote the grain growth, reducing oxygen vacancies, and influenced the tension between the new interfaces of the subsequent layer of BFO, thereby altering the physical and chemical properties obtained in the heterostructure. These show the coexistence of ferroelectricity and magnetism in the material. Measurements of capacitance and electrical polarization as a function of the magnetic field have been made and have indicated the magnetic–electric coupling at room temperature with high dielectric constant. Such materials may be of great significance in basic as well as applied research.

✉ A. Z. Simões
drleandrosrr@gmail.com

[1] Faculty of Engineering of Guaratinguetá, São Paulo State University - UNESP, Av. Dr Ariberto Pereira da Cunha 333, Bairro Pedregulho, Guaratinguetá, P.O. Box 355, SP 12.516-410, Brazil

[2] Interdisciplinary Laboratory of Electrochemistry and Ceramics, LIEC - Chemistry Institute, São Paulo State University - UNESP, Prof. Francisco Degni Street, 55, Quitandinha, Araraquara, SP 14800-060, Brazil

1 Introduction

During the last decade, the search for new magnetoelectric (ME) multiferroics capable of operating at room temperature has been the subject of intensive researches motivated, in particular, by the dream of realizing magnetically readable and electrically writable data storage systems [1–3]. In spite of continuous efforts, $BiFeO_3$ still remains to date the most promising room-temperature single-phase ME multiferroic [4]. Recently, electric control of the magnetization has been demonstrated in $BiFeO_3$ [5] but, still, the identification of alternative systems suitable for practical applications remains a real challenge. $BiFeO_3$ belongs to the family of multifunctional ABO_3 perovskite compounds that exhibit a wide variety of physical properties—such as ferroelectricity, piezoelectricity, (anti)ferromagnetism, colossal magnetoresistance, superconductivity, and spin-dependent transport—and have already led to numerous technological applications in electronics, optoelectronics, sensing, and data storage [6–8].

Initially restricted to simple cubic perovskites and solid solutions, the interest of the researchers recently extended to artificially or naturally layered perovskite compounds, that can host even more exotic phenomena [9, 10]. In 2008, a new type of improper ferroelectricity, arising from an unusual trilinear coupling between one ferroelectric (FE) and two antiferrodistortive (AFD) motions, was reported in $PbTiO_3/SrTiO_3$ superlattices (SLs) [11]. Since then, the coupling of lattice modes in perovskite layered structures has generated increasing interest [12]. The concept of "hybrid improper ferroelectricity" has been introduced [13] and rationalized, [14], guiding rules to identify alternative hybrid improper ferroelectrics have been proposed [15], and the emergence of ferroelectricity in rotation-driven ferroelectrics was discussed [16]. First synthesized in

the late 1950s by Kiselev et al. [17, 18], BFO was shown to be a G-type antiferromagnet with a Néel temperature of 630 K. Later, Sosnowska et al. [19] showed that the magnetic order of bulk BFO is not strictly collinear and that a cycloidal modulation with a period of 62 nm is present.

Although some methods have been used to decrease the current density leakage of BFO thin films, their electrical behavior is still not ideal [20–23]. It had been suggested that the trilinear coupling between FE and AFD structural degrees of freedom observed in $PbTiO_3/SrTiO_3$ SLs might be a convenient way to tune the magnetoelectric response in related magnetic systems. Subsequently, Benedek and Fennie reported an unprecedented electric field control of the magnetization in $Ca_3Mn_2O_7$, a naturally occurring Rudlesden–Popper layered compound in which a similar trilinear coupling of lattice modes can likely mediate an electric-field switching of the magnetization. This mechanism has not yet been confirmed experimentally, but appears as one of the most promising ways to achieve strong magnetoelectric coupling. In $Ca_3Mn_2O_7$, however, the magnetic order disappears at low temperature. Among the existing possibilities, the structure layer by layer, referred to as heterostructure in which one of the layers is a ferroelectric BFO may be a more promising method for decreasing the leakage current density and improving the electrical properties. The bilayered thin films consisting of BFO and one other ferroelectric layer have been reported [21–23], such as $Bi_{1/2}Na_{1/2}TiO_3$, $Pb(Zr,Ti)O_3$. Some interesting results have been demonstrated by such a bilayered structure, such as the improvement in phase purity, reduction in current density leakage, and the enhancement in fatigue behavior, but still their polarization value is much lower as compared with the intrinsic polarization of BFO thin films.

The ferrite lanthanum, $LaFeO_3$, is a perovskite oxide with semi-conducting behavior [24], This oxide crystallizes in an orthorhombically distorted perovskite structure with anti-ferromagnetic characteristics [25]. The particular characteristics of anti-ferromagnetism and an extremely high ordering temperature (T_N) are very promising for the use of the material in the storage industry, gas sensors, electrode material in solid-state fuel cells (SOFC), in spin valves, in exchange bias applications and in heterostructures of magnetic/magnetic and magnetic/electric films [26–30]. The magnetoelectric (ME) coefficient $\alpha ME = dE/dH = dV/(tdH)$ is the most critical indicator for the magnetoelectric coupling properties in multiferroic materials, where V is the induced magnetoelectric voltage, H is the exciting ac magnetic field, and t is the thickness of the sample used for measuring V across the laminate [30]. Among the various approaches to improve the magnetoelectric coupling in BFO thin films, these can be combined with an antiferromagnetic (AFM) layer consisting of $LaFeO_3$ (LFO). Thus, this heterostructure, becomes a promising candidate to improve the coupling between the magnetic and polarization states of the BFO.

AFM layer films play an important role to the functioning of magnetoelectric devices, in which serve to pin an adjacent layer ferromagnetic (FM) through force of the exchange-bias coupling [31]. The interest in exchange-biased nanostructures has accelerated recently, as a result of advances in fabrication methods and the emergence of novel tools for characterization of magnetic and electrical properties with high spatial resolution. Theoretical models describing exchange-bias recognize the formation of domains in the antiferromagnet as being important to the strength of the exchange coupling. The mechanism responsible for domain formation is not as straightforward as in the case of ferromagnets, since there is no macroscopic demagnetizing field. The fact that a multidomain configuration is usually observed in antiferromagnets is commonly explained by domain stabilization due to lattice imperfections, such as crystalline twins, dislocations, and interstitial atoms. Distortions of the crystalline structure, e.g., due to epitaxial strain, couple to the magnetic order parameter through magnetoelastic effects and are believed to play a key role in the AFM domain formation. The AFM domains are of particular importance to exchange-biased thin film nanostructures comparable in size on the exchange coupling by domain formation in the antiferromagnet. Although many researches exist on magnetic domain formation in FM nanostructures, less is known about the formation of antiferromagnetic domains of nanoscala heterostructures.

In the present work, the bilayered thin films consisting of $BiFeO_3$ and $LaFeO_3$ were grown on $Pt/TiO_2/SiO_2/Si$ (100) substrates by the chemical solution deposition method. The dependent relationship between the magnetoelectric co-efficient on magnetic field is still little explored in the literature. The magnetic and dielectric properties of these heterostructures crystallized by the polymeric precursor method were investigated for reasons that $LaFeO_3$ shows chemical heterogeneity and antiferromagnetism at room temperature, thus can result in tension between the LFO/BFO interface, and thus formation of this may optimize the physical properties and be of great relevance for applications in engineering devices.

2 Experimental procedure

The thin films were prepared using the polymeric precursor method, as described elsewhere [32]. Iron(III) nitrate nonahydrate (Aldrich), bismuth(III) nitrate pentahydrate (Aldrich), and lanthanum(III) nitrate hexahydrate (Aldrich)

were used as raw materials. The polymeric solution was prepared at a molar ratio of metal:citric acid:ethylene glycol of 1:4:16. All reagents have analytical purity. The precursor iron solution was prepared by dissolution of $Fe(NO_3)\cdot 9H_2O$ (Aldrich) in aqueous citric acid solution under stirring, and thus the temperature was increased to 90 °C for the formation of metal chelates. Similar procedure was used to obtain the other solutions. Later, the polymer precursor solutions were stechiometrically mixed to obtain the bismuth ferrite (BFO solution) and to obtain the lanthanum ferrite (LFO solution). After homogenization, the solution temperature was increased to 100 °C and ethylene glycol was added to achieve polymerization of the solution. The solution viscosity was adjusted to 21 cP by controlling the deionized water content using a Brookfield viscometer (Model—LV-DV3T). The solution layers were deposited on $Pt/Ti/SiO_2/Si$ substrates by spin coating (spin coater KW-4B, Chemat Technology) operating at 5000 rpm for 30 s. Then, the films were annealed at 300 °C for 1 h, using a heating rate of 3 °C/min in conventional furnace, to remove organic material. After the pre-firing, each layer was crystallized in a conventional furnace under static air at 500 °C/2 h for BFO films and 550 °C/2 h for LFO films, both using a heating rate of 5 °C/min. This process was repeated 10 times for films BFO, LFO, and five times of each material for the formation of heterostructured substrate/LFO/BFO film, with a total of 10 layers, as shown in the diagram of Fig. 1ii.

Phase analysis of the films was performed at room temperature from X-ray diffraction (XRD) patterns recorded on a Rigaku-DMax 2000PC with Cu-Kα radiation in the 2θ range from 20° to 60° with 0.3°/min steps. The annealed thin film thickness was determined using scanning electron microscopy (SEM) (Topcom SM-300) by checking the cross-section where back-scattered electrons were utilized. Three measurements were taken to obtain an average thickness value. In order to do the magnetic and electrical measurements Pt electrodes were deposited on top of the films. After deposition of the top electrode, the film was subjected to a post-annealing treatment in a tube furnace under an oxygen atmosphere at 300 °C for 1 h. Here, the desired effect was to eventually decrease present oxygen vacancies. The J–V measurements were carried out at room temperature and recorded on the Radiant Technology tester in the current-voltage mode, with a voltage change from 0 to +10 V, from +10 to −10 V and back to 0 V with a voltage step width of 0.1 V and elapsed time of 1.0 s for each voltage. The hysteresis loop measurements were carried out on the films with a Radiant Technology RT6000HVS at a measured frequency of 60 Hz. These loops were traced using the Charge 5.0 program included in the software of the RT6000HVS in a virtual ground mode test device. The magnetoelectric coefficient measurements in the films were attained in a dynamic lock-in technique. Additionally, an ac magnetic field up to 10 Oe with frequency of 7 kHz was superimposed onto the dc field. The ac field was produced by a Helmholtz-type coil (180 turns witha diameter of 50 mm), driven by an ac current generated by a function generator (Philips PM5192). The amplitude of the ac field was calculated from the driving current measured by a multimeter (Keitley 196 System DMM). The dc magnetic bias field was produced by an electromagnet (Cenco Instruments J type). The time-varying dc field was achieved by a programmable dc power supply (Phillips PM2810 60 V/5 A/60 W). A Hall probe was employed to measure the dc magnetic field. Magnetization measurements were done by using a vibrating-sample magnetometer (VSM) from Quantum Design™. The magnetoelectric signal was measured by using a lock-in amplifier (EG&G model 5210) with input resistance and capacitance of 100 MΩ and 25 pF, respectively.

Piezoelectric measurements were carried out using a setup based on an atomic force microscope in a Multimode Scanning Probe Microscope with Nanoscope IV controller (Veeco FPP-100). In our experiments, piezoresponse images of the films were acquired in ambient air by applying a small ac voltage with an amplitude of 2.5 V (peak to peak) and a frequency of 10 kHz while scanning the film surface. To apply the external voltage we used a standard gold coated Si_3N_4 cantilever with a spring constant of 0.09 N/m. The probing tip, with an apex radius of about 20 nm, was in mechanical contact with the uncoated film surface during the measurements. Cantilever vibration was detected using a conventional lock-in technique.

3 Results and discussion

Figure 1 shows the results of structural and morphological analysis of the obtained films. In Fig. 1i shows the XRD patterns of thin films prepared in this work. The Fig. 1ia shows the diffraction peaks for LFO film crystallizes in a distorted antiferromagnetic perovskite orthorhombic structure with a space group Pbnm according to the JCPDS 74-2203 card in which all planes were indexed. The diffraction peaks for BFO film (Fig. 1ib) can be indexed through a rhombohedral structure with a space group R3c according to the JCPDS 71-2494 card in which too all planes were indexed. The Fig. 1ic shows the diffraction peaks for LFO/BFO heterostructure film in which the spectrum can be separated in two sets of well-defined peaks, one of which belongs to the perovskite BFO and the other to the LFO, showing that there was no diffusion between the different layers of the present films. All films were shown polycrystalline without specific orientation, with pure perovskite phase. The crystal sizes of the phases

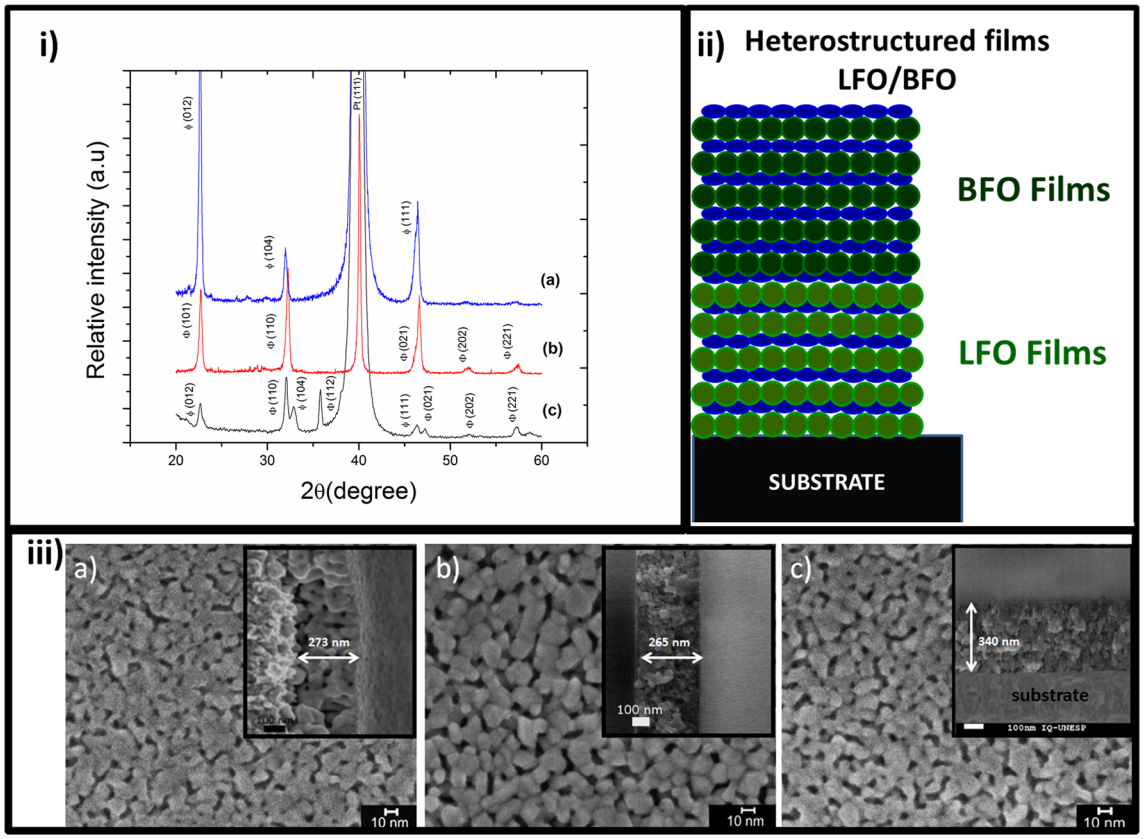

Fig. 1 **i** X-ray diffraction of thin films, deposited by the polymeric precursor method: *a* LFO, *b* BFO and *c* LFO/BFO; **ii** diagram LFO/BFO heterostructure films; **iii** FEG-SEM images of surface and cross section of thin films deposited: *a* LFO; *b* BFO and *c* LFO/BFO

involved were calculated using the Debye–Scherrer equation, which gave a crystal size of 24, 37 and 40 nm for the BFO, LFO, and LFO/BFO films, respectively. These results reveal that the contribution to the crystal size of the BFO in the heterostructure is significant through the insertion the underlayer LFO. It is important to note that diffraction peak of LFO thin film at (112) was visible in the X-ray pattern of the LFO/BFO multilayered system. This may have been due to the relatively higher intensity diffraction peak resulting from the grain size and thickness of the alternate layers of LFO and BFO thin films. These findings indicate that the proposed methodology allows for the deposition of multilayer heterostructures without diffusion at the interfaces of adjacent LFO–BFO layers as depict in Fig. 1ic. It can be considered that the thinner layers of singular films are significantly affected by the crystallographic orientation of the underlying layer. Thinner films present large amount of defects associated to the disorder in the lattice. The disorder developed in the film is strongly dependent on the thickness showing that the amount of material deposited on the surface of substrate causes a reduction in the defects or disorder of materials. Therefore, both BFO and LFO films deposited on platinum coated silicon substrates have less peaks compared to the multilayered film because in this plane the interatomic distances of the material and substrate are very close [28]. The Fig. 1ii shows the arrangement in which the layers of heteroestruturados films were obtained.

Changes on the surface morphology of the thin films were evaluated by FEG-SEM measurements and the thicknesses of the films are shown in the insets of Fig. 1iii. Among these films, the single-layered LFO thin film (Fig. 1iiia) exhibits a smooth surface and homogeneous interconnected grain size distribution, with average grain size of 10 nm, and low porosity. In comparison the BFO film (Fig. 1iiib) present an inhomogeneous microstructure, composed small and larger grains with average grain size of 10 and 25 nm, respectively, and high porosity. The heterostructure film (Fig. 1iiic) consists of grains with homogeneous particle size distribution, with an average grain size of 15 nm. Comparing the films, it can be seen that the heterostructured film tends to suppress the porosity and exhibited the most homogeneous microstructure, indicating that the bottom LFO layer, in the heterostructure, was able to suppress the grain growth of BFO during the annealing process. The annealing temperature and

coupling between two layers was found to be effective in improving the surface morphology of synthesized film, because the precursor film underwent the optimized nucleation and growth process producing films with a homogeneous and dense microstructure, as can be seen in the inset of Fig. 1iiic the cross section of heteroestruturados films. Also, the homogeneous microstructure of such film may affect the leakage properties, because the voltage can be applied uniformly onto it. In this way, we observed that addition of LFO sublayer strongly influenced the microstructure, inhibiting grain growth of BFO which is the active ferroelectric phase.

The leakage currents density as a function of voltage is shown in the Fig. 2. The measured logarithmic current density (log J) versus the voltage (V) is symmetric and shows two clearly different regions. The current density increases linearly with the external voltage in the region of low applied voltage strengths which suggests an Ohmic conduction. The insulating properties of the films were found be dependent on the microstructure of singular films and of the heterostructured films. The leakage current density it is lower for the LFO and heterostructured film as compared to pure BFO layer, we can observe it the 5.0 V in which the leakage current density changes from 10^{-4} A/cm^2 (BFO) to 10^{-8} A/cm^2 (LFO) and 10^{-6} (BFO–LFO). One reason for this is that introduction of LFO sublayer reduces grain sizes of the BFO film as evidenced by FEG-SEM, leading to an increase in the density of grain boundaries, which makes contribution to the decreased leakage current density [29]. Another reason is that the decreased Bi volatilization and the restrained reduction of Fe^{3+} to Fe^{2+} are realized by virtue of the reducible oxygen vacancies and cation defects after LFO insertion. Normally, the mobile oxygen vacancies are donor like trapping centers for electrons. The energy levels associated with $(V_{O_2^-})^{\cdot\cdot}$ are very close to the conduction band. Therefore,

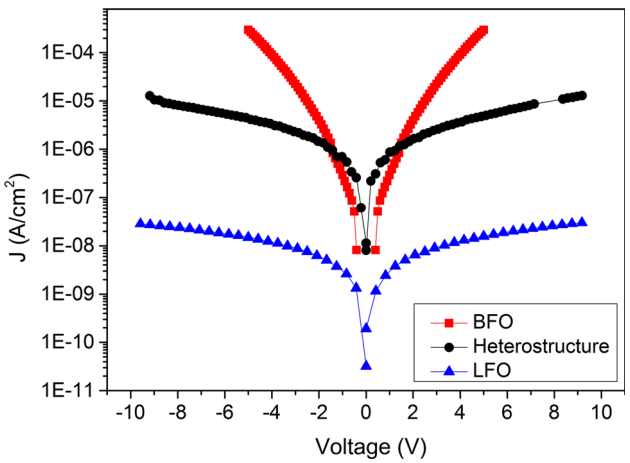

Fig. 2 Leakage current density versus applied voltage of thin films

the electrons can be readily activated to be free for conduction by the electric field. However, the electric field required for generating the free electrons in BFO-based film may be increased if the defect complexes between the $(V_{O_2^-})^{\cdot\cdot}$ are formed, since the applied electric field has to overcome the electrostatic attraction force between $(V_{O_2^-})^{\cdot\cdot}$ and $(V_{Bi}^{'''})$ before the oxygen vacancies become mobile and can serve as the trapping centers for electrons. Note that the different positions occupied by $(V_{O_2^-})^{\cdot\cdot}$ in perovskite octahedral will result in different electrostatic forces between $(V_{Bi}^{'''})$ and $(V_{O_2^-})^{\cdot\cdot}$, which in turn lead to that the different electric fields will be required for breaking the defect complexes. Based on the above discussion, the high leakage current in BFO film compared to that in LFO film may result from the formation of defect complexes between $(V_{Bi}^{'''})$ and $(V_{O_2^-})^{\cdot\cdot}$. Thus, the increase of the leakage current with the electric field can be ascribed to the gradual release of $(V_{O_2^-})^{\cdot\cdot}$ from the complexes of $(V_{Bi}^{'''}) - (V_{O_2^-})^{\cdot\cdot}$. This study demonstrates that the microstructures of ferroelectric films play an important role in their conductivity properties [30]. Thus for higher field strengths, the current density increases exponentially which implies that at least a part of the conductivity results, derives from emission mechanism Schottky or Poole–Frenkel.

In order to analyze the dominant mechanism in the multilayered films at higher fields, the J–E properties were plotted using Schottky and Poole–Frenkel (P–F) emission models (Figs. 3a, 4b, respectively). The former is a Schottky emission (SE) process across the interface between a semiconductor (metal) and an insulating film as a result of barrier lowering due to the applied field and the image force. The latter is associated with the field enhanced thermal excitation of charge carriers from traps, sometimes called the internal Schottky effect. These two transport mechanisms are very similar and can be distinguished from the slope measured from the straight line region of the current–voltage (I–V) curve in the form of $\log_{10}(J)$ or $\log_{10}(J/E)$ versus $E^{1/2}$plots, respectively. Schottky emission (Fig. 3a) plots for multi-layered films deposited indicate good linearity by least square fit, suggesting that the leakage current mechanism is governed by such mechanism. On the other hand, multilayered film has no linearity by least square fit indicating that Poole–Frenkel (Fig. 3b) mechanism is absent. This can be explained by consume of concentration variation of the oxygen vacancies in the films. In this region, the injection of charge carriers in the film takes place. As the applied voltage is increased further, very strong injection of charge carriers takes place, and causes an increase in the density of filled trapping sites. If sufficient charge is injected into the insulator, all the traps will become filled. Further injected charge then exists as free charge in the conduction band

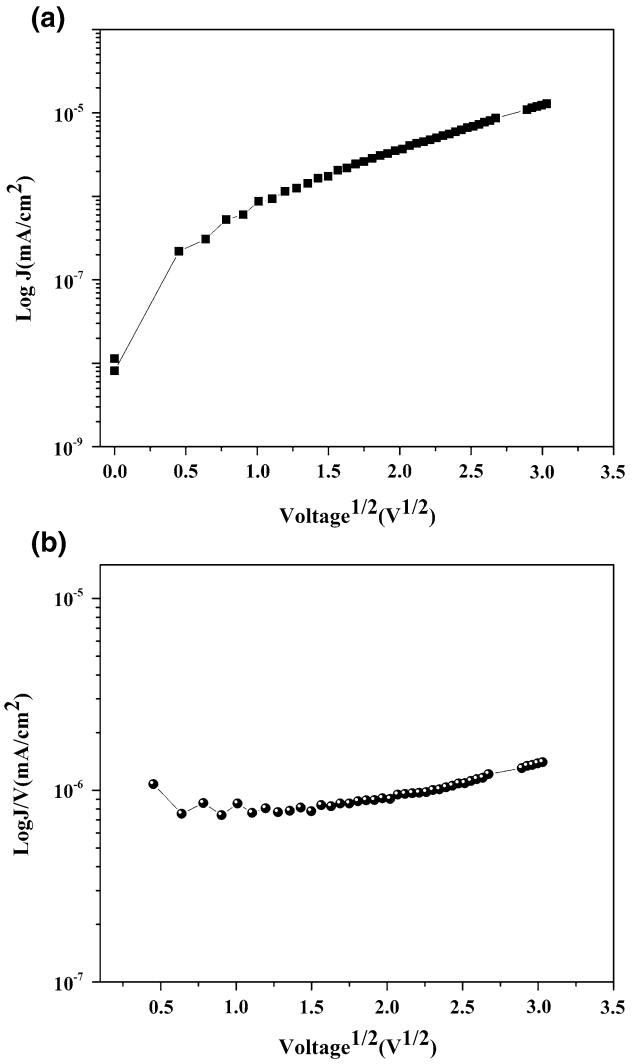

Fig. 3 **a** The Schottky log (J) and **b** the P–F log (J/V) relationships are plotted as a function of $V^{1/2}$ for multilayered film

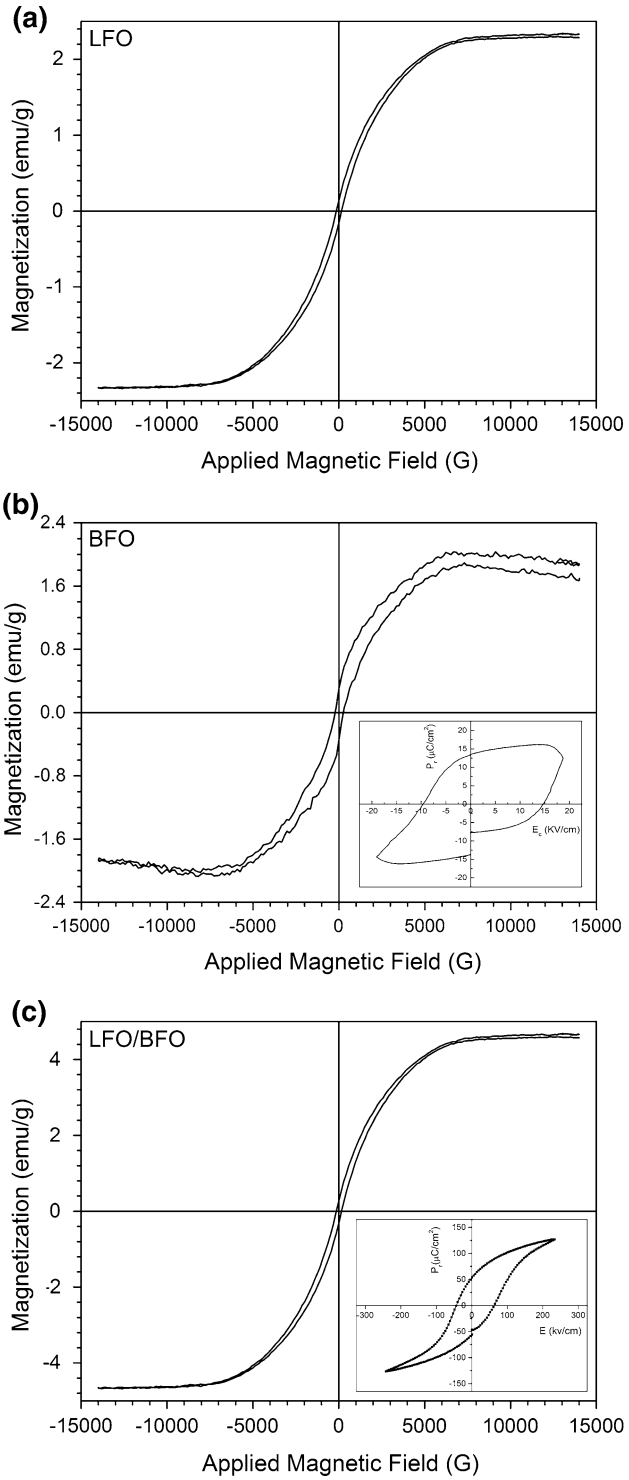

Fig. 4 Field dependencies of the magnetization obtained of thin films: **a** LFO; **b** BFO and **c** LFO/BFO and *inset* P–E hysteresis loop of thin films

and contributes to the current. In the multilayered structure, carrier injection into the insulator looks very important, so space charge can distribute along the grain boundaries and the traps in high fields are consumed inhibiting the origin of the nonlinear behavior. Therefore, the predominant mechanism can be considered as Schottky type.

The magnetic properties of the films at room temperature are shown in the magnetization versus applied magnetic field plots in the Fig. 4. The magnetic hysteresis loops of the single-layered LFO and BFO film and the heterostructure LFO/BFO were normalized by the volume fraction of the films layers, all films exhibit well-defined hysteresis loops with a saturation magnetization (M_s) of 2.3, 1.9 and 4.7 emu/g, respectively. The coercive fields (2Hc) of the films: LFO, BFO and LFO/BFO heterostructures, are 158, 256 and 153 Gauss, respectively. The ferromagnetic response suggests that the magnetic behavior is influenced by the crystal size as M_s has been reported to drop according with the reduction in the crystal size [33–35]. Figure 4 shows too the P–E hysteresis loops of thin

films measured at room temperature. In inset Fig. 4b, c shows the P–E hysteresis loops of BFO and LFO–BFO thin films, respectively. Due the absence of hysteresis loop P–E in the LFO film no signal could be measured with the applied voltage and frequency. The film BFO shows a polarization value of 15.8 μC/cm^2 at an applied field of 10 V. This low value, compared to the sequential result of heterostructures, is not intrinsic but induced by high leakage in this structure, as indicated by the roundish shape of the P–E loop. Additionally, space charges can also contribute to the polarization property. A poor P–E hysteresis loop was observed, as has been typically observed from conductive ferroelectrics and its breakdown with increased bias electric field is due to a large leakage current. However, the heterostructured films LFO/BFO shows a well saturated and rectangular loop, with high Pr of 53 μC/cm^2 after applying a voltage of 10 V. For this film no sign of leakage has been observed under a measuring frequency of 60 Hz. Possibly, low coercive fields could be expected when the upper film layer is subjected for a long time annealing resulting high defect concentrations and higher leakage. For that reason new films are being prepared, as well as in our work with the insertion of $LaFeO_3$, with the function of bottom oxide electrode to minimize formation of oxygen vacancies between the sublayers, as has been reported substantial reduced of leakage current of $BiFeO_3$ films by introducing of $LaNiO_3$ used as bottom oxide electrode [31]. Another factor that increases the ferroelectricity is in relative displacement Bi ions by Fe–O octahedral, along the epitaxial orientation in thin films BFO. According to Wang et al. [36], projections polarization along directions (110) is greater than polarizations along orientation (100). In this direction our results are comparable to those observed in the epitaxial BFO films on a (100) $SrTiO_3$ substrate prepared by the pulsed layer deposition (PLD) method [37].

To visualize the domain structures of the LFO/BFO heterostructures thin films, we performed piezoelectric force microscopy (PFM) and the results are illustrated in Fig. 5. The out-of-plane (OP) and in-plane (IP) piezoresponse images of the as-grown films after applying a bias of −12 V, on an area of 2 μm × 2 μm, and then an opposite bias of +12 V in the central 1 μm × 1 μm area were employed. To obtain the domain images of the films, a high voltage that exceeds the coercive field was applied during scanning. The contrast in these images is associated with the direction of the polarization [38]. Topography is illustrated in Fig. 5a. The white regions in the out-of-plane PFM images correspond to domains with the polarization vector oriented toward the bottom electrode hereafter referred to as down polarization (Fig. 5b) while the dark regions correspond to domains oriented upward referred to as up polarization. Grains which exhibit no contrast change are associated with zero out-of-plane polarization. A similar behavior was observed when a positive bias was applied to the film. We noticed that some of the grains exhibit a white contrast associated to a component of the polarization pointing toward the bottom electrode. On the other hand, in the in-plane PFM images (Fig. 5c) the contrast changes were associated with changes of the in-plane polarization components. In this case, the white contrast indicates polarization e.g. in the positive direction of the y-axis while dark contrast are given by in-plane polarization components pointing to the negative part of the y-axis. The ferroelectric domains of our films consist of a multiple domain state in a mixture of 71° and 180° domains which grow large into blocks. That the domains grow in multiple states is the consequence of thickness of films being close to 300 nm. PFM measurements reveal a clear piezoelectric contrast corresponding to antiparallel domains on all locations tested. Local piezoresponse is approximately two times weaker as compared with undoped $BiFeO_3$ ceramics [39], pointing out a smaller value of the spontaneous polarization. There is no reduction in the amplitude of the measured vibrations for the highest doped film which is indicative that this phase is still polar and electric field-induced polarization switching still exists. Therefore, our data confirm that the spontaneous polarization is very high with addition of LFO sublayer. In this way, the LFO sublayer can reduce the strain energy and pin charged defects. This is a consequence of changes in grain boundary resistance for the multi-layered films which suggest low conductivity. In this way, lanthanum ferrite sublayer reduces the oxygen vacancies and as consequence improves the switching process of electrical dipoles. Pure BFO present defects as Bi or Fe vacancies resulting in an increase in conductivity. Therefore, this fact indicates the presence of mobile carriers which are positively charged and that the possibility of hopping through the Bi ion can be considered. Also, we noted that some of the crystallites apparently have not been switched and still exhibit a positive piezoresponse signal. This result, which can be explained by strong domain pinning in these crystallites, is direct experimental proof that repeated switching results information of unswitchable polarization, which, in turn, leads to the degradation of switching characteristics.

In order to demonstrate the coupling between electric and magnetic polarizations in LFO/BFO film, we have carried out two experiments, namely, (Fig. 6a) the measurement of electric polarization after poling the sample in a magnetic field, Fig. 6b in situ changes in capacitance with the application of a magnetic field. The change in saturation polarization (*Ps*) values for the sample after poling at different magnetic fields is illustrated. A continuous increase in *Ps* is seen with an increase in the poling field before *Ps* eventually saturates. This is indicative of

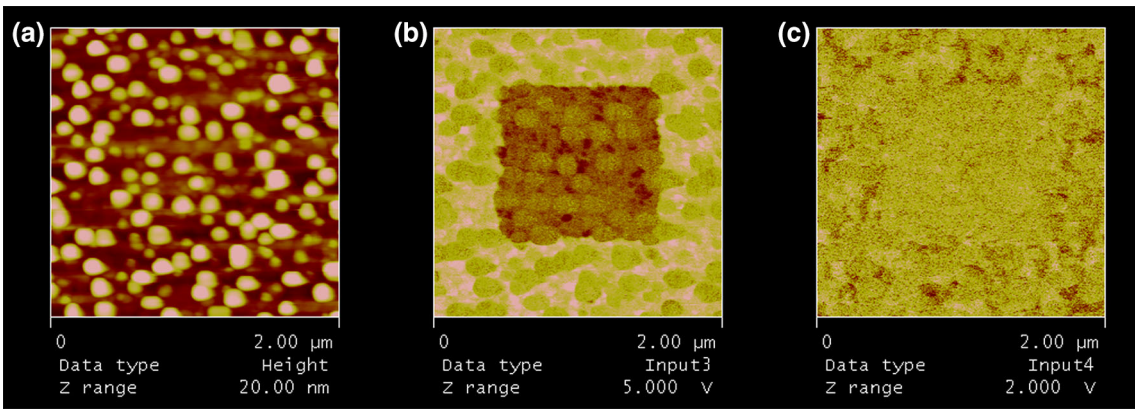

Fig. 5 Piezoresponse microscopy obtained of thin films: **a** topography; **b** out-of-plane and **c** in-plane

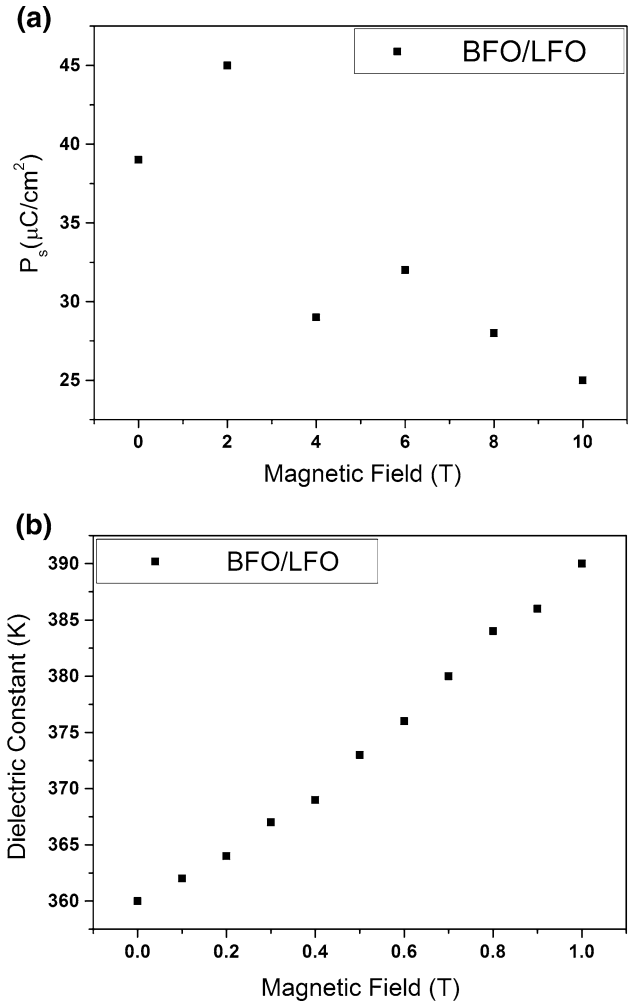

Fig. 6 Magnetic field as a function of **a** spontaneous polarization and **b** dielectric contant obtained of thin films LFO/BFO

the coupling between the two polarizations. An increase in the dielectric constant with an increase in the magnetic field is observed, and this is also a signature of the ME conversion occurring in the sample. The magnetoelectric coupling observed at room temperature may be envisaged as follows. When a magnetic field is applied to a magnetoelectric material, the material is strained. This strain induces a stress on the piezoelectric (all ferroelectrics are piezoelectric), which generates the electric field. This field could orient the ferroelectric domains, leading to an increase in polarization value. Such magnetoelectric coupling and the large dielectric constant observed in the present system could be useful in device applications.

The unipolar strain behavior at room temperature is shown in Fig. 7. The unipolar strain presents a maximum at 5 kV/cm while the saturation regime is reached at 10 kV/cm. Lanthanum ferrite affects the strain behavior in part due to domain reorientation. Beyond that point, it is possible that a modest bias field results in the transition from asymmetric to symmetric phase. This field-induced phase transition may be ascribed to the pinching effect, that is, the consequent decrease in free energy difference among polymorphic phases. A careful inspection of the S–E plots reveals that there are two apparent linear regions at low fields ($E < 5$ kV/cm) and high fields ($E > 10$ kV/cm) and one transition region, that corresponds to domains reorientation induced by external electric fields. The hysteretic strain could be associated with domain reorientation. The strain is hysteresis free at electric fields higher than 5 kV/cm, indicating a stable single domain/poling state induced by the high external electric fields. In addition, from the S versus E profiles, no noticeable induced phase transition is observed at such high electric fields. It is shown that the heterostructured film present a strain ($S = 0.001$ %) at 5 kV/cm). It is shown that lanthanum ferrite reduces the unipolar strain when compared to BFO films, i.e. the strain was ($S = 0.002$ %) for singular BFO films, respectively. The decreasing of both strain response and strain energy after doping process can be associated to the reduced polarizability and the pinning effect. As can be seen, the

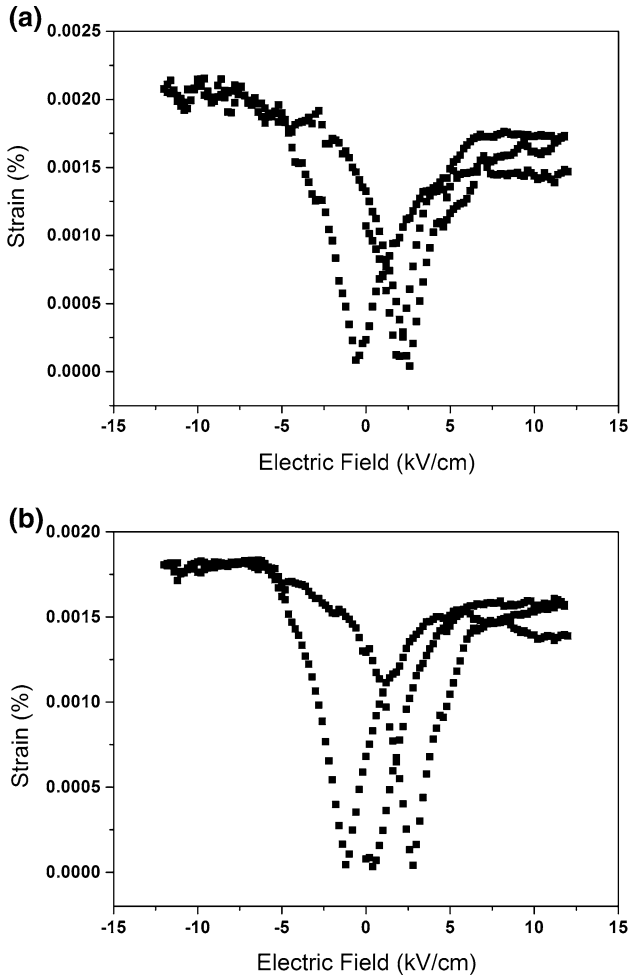

Fig. 7 Strain as a function of electric field obtained of thin films **a** BFO and **b** LFO/BFO

small strain variations one each curve with electric field can be probably caused by clamping effect due to the stress created in the film-substrate interface and the existence of an ultrathin air gap between the tip and the sample which might lower the actual voltage drop in the film.

4 Conclusions

Thin films of type heterostructured LFO/BFO has been successfully obtained by chemical method. The polycrystalline films showed good crystalline phases of BFO and LFO, and without the presence of secondary phases. Our results showed that the bottom layer film LFO has influenced the growth morphology of the up layer BFO films, as well as electrical and magnetic properties of the heterostructure compared the single layers. The heterostructures showed better remaining polarization and lower current density, in consequence of the LFO insertion on the grain boundary density, and oxygen vacancies. The high dielectric permittivity of the LFO/BFO was mainly due to less structural disorder and less two-dimensional stress in the plane of the film. In-plane magnetization-field curves revealed improvement of magnetization of the heterostructure which was influenced by the crystal size. The maximum strain measured for the LFO/BFO film was 0.001 % at 5 kV/cm. We have shown in this work the ferroelectricity, ferromagnetism weak, and magnetoelectric coupling states with high dielectric constant. Thus suggesting that such systems are promising candidates for achieving electrical switching of the magnetization at room temperature and thus a promising material to be used in different of electronic applications.

Acknowledgments The financial support of this research project was from the Brazilian research funding agencies CNPq 573636/2008-7, INCTMN 2008/57872-1 and FAPESP 2013/07296-2. We would like to thank Professor Elson Longo for facilities.

References

1. M. Muneeswaran, R. Dhanalakshmi, N.V. Giridharan, J. Mater. Sci. Mater. Electron. **26**, 3827–3839 (2015)
2. S. Thirumalairajan, K. Girija, V.R. Mastelaro, N. Ponpandian, J. Mater. Sci. Mater. Electron. **26**, 8652 (2015)
3. L. Luo, N. Jiang, F. Lei, Y. Guo, Q. Zheng, D. Lin, J. Mater. Sci. Mater. Electron. **25**, 1736 (2014)
4. C. Gao, P. Zhang, C. Zhang, D. Xue, Ceram. Int. **41**, S851 (2015)
5. G.A. Smolenskii, I.E. Chupis, Sov. Phys. Usp. **25**, 475 (1982)
6. M.M. Rashad, J. Mater. Sci. Mater. Electron. **23**, 882 (2012)
7. A. Shukla, R.N.P. Choudhary, J. Mater. Sci. Mater. Electron. **22**, 1222 (2011)
8. G.S. Pattanayak, R.N.P. Choudhary, P.R. Das, J. Mater. Sci. Mater. Electron. **24**, 2767 (2013)
9. W. Eerenstein, F.D. Morrison, J. Dho, M.G. Blamire, J.F. Scott, Science **307**, 1203 (2005)
10. X. Guo, Y. Wu, Y. Zou, Z. Wang, J. Mater. Sci. Mater. Electron. **23**, 1072 (2012)
11. A. Vasudevarao et al., Phys. Rev. Lett. **97**, 257602 (2006)
12. K. Kato, S. Lida, J. Phys. Soc. Jpn. **51**, 1335 (1982)
13. Y. Yamasaki et al., Phys. Rev. Lett. **96**, 207204–207206 (2006)
14. M. Gajek et al., Nat. Mater. **6**, 296 (2007)
15. W.J. Gallagher, S.S.P. Parkin, IBM J. Res. Dev. **50**, 5 (2006)
16. M. Dawber, K.M. Rabe, J.F. Scott, Rev. Mod. Phys. **77**, 083 (2005)
17. P. Royen, K. Swars, Angew. Chem. **24**, 779 (1957)
18. S.V. Kiselev, R.P. Ozerov, G.S. Zhdanov, Sov. Phys. Dokl. **7**, 742 (1963)
19. I. Sosnowksa, T. Peterlin-Neumaier, E. Steichele, J. Phys. C **15**, 4835 (1982)
20. J.G. Wu, G.Q. Kang, H.J. Liu, J. Wang, Appl. Phys. Lett. **94**, 172906 (2009)
21. J.G. Wu, G.Q. Kang, J. Wang, Appl. Phys. Lett. **95**, 192901 (2009)
22. H. Béa, M. Bibes, S. Fusil, K. Bouzehouane, E. Jacquet, K. Rode, P. Bencok, A. Barthélémy, Phys. Rev. B **74**, 020101(R) (2006)
23. D. Xie, Y. Zang, Y. Luo, X. Han, T. Ren, L. Liu, J. Appl. Phys. **105**, 084109 (2009)

24. E. Traversa, S. Matsushuma, G. Okada, Y. Sadaoka, Y. Sakai, K. Watanabe, Sens. Actuator B-Chem. **24**, 661 (1995)
25. D. Kuscer, M. Hrovat, J. Holc, S. Bernik, D. Kolar, J. Power Sources **61**, 161 (1996)
26. N.N. Toan, S. Saukko, V. Lantto, Phys. B **327**, 279 (2003)
27. R. Dogra, A.C. Junqueira, R.N. Saxena, A.W. Carbonari, J.M. Filho, M. Moralles, Phys. Rev. B **63**, 224104 (2001)
28. A. Scholl, J. Stohr, J. Luning, J.W. Seo, J. Fompeyrine, H. Siegwart, J.P. Locquet, F. Nolting, S. Anders, E.E. Fullerton, M.R. Scheinfein, H.A. Padmore, Science **287**, 1014 (2000)
29. X. Qi, J. Dho, R. Tomov, M.G. Blamire, J.L. MacManus-Driscoll, Appl. Phys. Lett. **86**, 062903 (2005)
30. Y. Wang, C.W. Nan, J. Appl. Phys. **103**, 024103 (2008)
31. H. Liu, Z. Liu, K. Yao, J. Sol-Gel, Sci. Technol. **41**, 123 (2007)
32. A.Z. Simões, M.A. Ramirez, C.S. Riccardi, E. Longo, J.A. Varela, Mater. Lett. **60**, 2020 (2006)
33. M.M. Kumar, S. Srinath, G.S. Kumar, J. Magn. Magn. Mater. **188**, 203 (1998)
34. T. Kanai, S.I. Ohkoshi, A. Nakajima, K. Hashimoto, Adv. Mater. **13**, 487 (2001)
35. C.S. Liang, J.M. Wu, M.C. Chang, Appl. Phys. Lett. **81**, 3624 (2002)
36. Y. Wang, C.W. Nan, Appl. Phys. Lett. **89**, 052903 (2006)
37. C.D. Pham, J. Chang, M.A. Zurbuchen, J.P. Chang, Chem. Mater. **27**, 7282 (2015)
38. A.Z. Simões, A.H.M. Gonzalez, L.S. Cavalcante, C.S. Riccardi, E. Longo, J.A. Varela, Appl. Phys. Lett. **90**, 052906–052908 (2007)
39. V.V. Shvartsman, W. Kleemann, R. Haumont, J. Kreisel, Appl. Phys. Lett. **90**, 172115–172117 (2007)